Colloid Polym Sci (2015) 293:2201–2208
DOI 10.1007/s00396-015-3614-8

ORIGINAL CONTRIBUTION

Electrospinning preparation, thermal, and luminescence properties of $Eu_2(BTP)_3(Phen)_2$ complex doped in PMMA

Huiquan Gu[1] · **Yanjun Hou**[1] · **Feng Xu**[1] · **Shuhong Wang**[2]

Received: 20 January 2015 / Revised: 18 April 2015 / Accepted: 27 April 2015 / Published online: 3 May 2015

Abstract Different concentrations of bis-β-diketonate complex $Eu_2(BTP)_3(Phen)_2$ (BTP=1,3-bis(4,4,4-trifluoro-1,3-dioxobutyl)-phenyl and Phen=1,10-phenanthroline) were doped into the poly(methylmethacrylate) (PMMA), forming a series of red Eu/PMMA luminescent nanofibers, via electrospinning technology. Various characterization techniques were employed to reveal the effect of $Eu_2(BTP)_3(Phen)_2$ on the morphology, thermal stability, and luminescence of composite nanofibers. FT-IR spectra show the $Eu_2(BTP)_3(Phen)_2$ complex was successfully doped into PMMA. The luminescent spectra of the composite nanofibers show strong characteristic emission of Eu^{3+} ions. Simultaneously, in comparison with the precursor complex $Eu_2(BTP)_3(Phen)_2$, the Eu/PMMA nanofibers has a great improvement in thermal stability. Furthermore, the Judd-Ofelt theory and simulative constructions of the complex are employed to explain the effect of the dispersion of $Eu_2(BTP)_3(Phen)_2$ and the interactions between the $Eu_2(BTP)_3(Phen)_2$ complex and neighboring chain segments of PMMA.

Keywords Luminescent nanofibers · Electrospinning · Lanthanide complex · Judd-Ofelt analysis

Introduction

Lanthanide ions have attracted considerable interest because of their technological applications in amplifiers for optical communications, optoelectronic, supramolecular, and luminescent probes for biological system and sensor uses [1]. However, the main disadvantage of lanthanide ions may be their low extinction coefficients owing to the parity-forbidden nature of the inner-shell f→f transition, necessitating the incorporation of chelating ligands that are strongly absorbing in a process appropriately named the antenna effect [2]. Ideal antenna ligands must be able to harvest light efficiently and have a suitable T_1 energy for efficient energy transfer to the emissive state of the Ln^{3+} ions [3]. Many antenna ligands have been developed for lanthanide complexes [4]. Among the widely known ligands, the bis-β-diketonate ligand is one of the important "antennas" which can effectively transfer the intramolecular energy to the central ion [5]. However, another drawback of lanthanide ions may be the efficient nonradiative deactivation of their excited states by high energy oscillators such as O-H bonds from solvent molecules (H_2O) [6]. In order to overcome this deficiency and improve the characteristics of light emission, the solvent molecules were replaced by the ancillary nitrogen ligands such as Phen, which has a high efficiency of light absorption [7]. Additionally, the lanthanide complexes also display weak mechanical properties and low thermal stability in their original state, which limited their applications in the fabrication of optical materials [8]. Hence,

Electronic supplementary material The online version of this article (doi:10.1007/s00396-015-3614-8) contains supplementary material, which is available to authorized users.

✉ Yanjun Hou
houyj@hlju.edu.cn

✉ Shuhong Wang
openair@163.com

[1] Key Laboratory of Chemical Engineering Process and Technology for High-Efficiency Conversion, School of Chemistry and Materials Science, Heilongjiang University, Harbin 150080, People's Republic of China

[2] Key Laboratory of Functional Inorganic Material Chemistry School of Chemical Engineering and Material, Heilongjiang University, Ministry of Education, Harbin 150080, People's Republic of China

the complex will be incorporated into a matrix such as polymers to improve thermal stability and mechanical properties [9]. It is widely known that PMMA, one of the most ideal candidate, provides a series of advantages for the development of molecular materials, for instance, thermal and chemical stability, flexibility, versatility and biocompatibility, which can also influence the characteristic luminescence of Eu^{3+} ions [10, 11].

In addition, one-dimensional (1D) nanostructures have attracted tremendous interest in recent years due to their chemical, optical, and electrical properties [12]. By reducing the number of defects per unit length, a 1D nanostructure can render strong mechanical property that is essential for its nanoscale manipulation and further macro applications [13]. 1D nanostructures can be prepared by many methods such as template-directed methods [14], vapor-phase methods [15], self-assembly [16] and electrospinning [17], etc. Among the large number of fabrication methods demonstrated to generate 1D nanostructures, electrospinning has attracted rapidly increasing attention as a straightforward and simple method for forming inorganic superfine nanofibers from a polymer/inorganic composite precursor [18]. In the present work, the new complex/polymer composite material formed from the bis-β-diketonate Eu^{3+} complex were electrospun to form 1D nanofibers which will lead to significant flexibility, excellent optical properties, and thermal stability [19].

In this paper, a series of $Eu_2(BTP)_3(Phen)_2$/PMMA nanofibers were successfully prepared through electrospinning. The effect of $Eu_2(BTP)_3(Phen)_2$ on the morphology and luminescence of composite nanofibers has been studied. The luminescent properties of the nanofibers were investigated in comparison with that of the precursor complex. The effect of the dispersion of $Eu_2(BTP)_3(Phen)_2$ and the interactions between the $Eu_2(BTP)_3(Phen)_2$ molecules and neighboring chain segments of PMMA was also studied by the use of the Judd-Ofelt theory.

Experimental section

Materials and solution properties

Poly (methyl methacrylate) (PMMA M_w=120 000) was obtained from Tianjin Chemical Reagent Factory Damao (China). *N*,*N*-dimethylformamide (DMF) purchased from Tianjin Chemical Reagent Factory (China) was used as a solvent to prepare the electrospinning solution. Europium oxide (Eu_2O_3, 99.99 %) and sodium hydride (60 %, A. R.) were purchased from Helire (Shanghai, China) and Tianjin Chemical Reagent Factory (China), respectively.

$EuCl_3{\cdot}6H_2O$ and $Eu_2(BTP)_3(Phen)_2$ complex were prepared according to procedure previously described [20, 21]. $EuCl_3{\cdot}6H_2O$ was synthesized by dissolving lanthanide oxide in a slight excess of hydrochloric acid. The spinning solutions were prepared by first dissolving PMMA in DMF solution at the concentration of 18 wt% at ambient temperature. Subsequently, the $Eu_2(BTP)_3(Phen)_2$ complexes were added (contents of $Eu_2(BTP)_3(Phen)_2$ to PMMA equal to 5, 7, 9, 11, 13, and 15 wt%) into the above mixture solution and stirred for 6 h at 50 °C.

Preparation of luminescent nanofibers

The solutions were then placed into 1-mL plastic syringes attached to a stainless-steel needle with inner diameter of 0.37 mm. The electrospinning setup with a DC high-voltage generator was purchased from the BMEI Co., Inc. In the preparation of $Eu_2(BTP)_3(Phen)_2$/PMMA nanofibers, the voltage applied was 13 kV, and the distance between the collector and the tip of the needle was 20 cm. The nanofibers were collected as randomly overlaid mats on an electrically grounded aluminum foil. After electrospinning, the composite nanofiber mats were dried in a vacuum oven at room temperature for 12 h before characterizations.

Characterization

SEM image of the electrospinning nanofibers was obtained through the scanning electron microscopy (SEM) (Hitachi S-4800) working at 20 kV of acceleration voltage. Prior to SEM examination, the specimens were sputter-coated with gold to avoid charge accumulation. FT-IR spectral data were recorded on a PerkinElmer Spectrum One spectrophotometer in the range of 4000–400 cm^{-1} using KBr disks. Fluorescence microscope of Leica DM400 M with camera shot Leica DFC 425C was employed to study the luminescence of the composite nanofibers. Thermal analyses were conducted on a PerkinElmer STA 6000 with a heat in grate of 10 °C min^{-1} in a temperature range from 30 to 800 °C under atmosphere. Excitation and emission spectra were measured with an Edinburgh FLS 920 fluorescence spectrophotometer. Luminescence lifetimes were recorded on a single photon counting spectrometer from Edinburgh Instrument (FLS 920) with microsecond pulse lamp as the excitation source. The data were analyzed by software supplied by Edinburgh Instruments. Both the slit widths for excitation and emission were set at 2.0 nm. The fluorescence dynamics of the samples were measured with an FLS 920 instrument (Edinburgh). During the measurements, an oscillograph was used to record the decay dynamics, and the 335 nm incident light generated from a microsecond flash lamp, which was used as the excitation source.

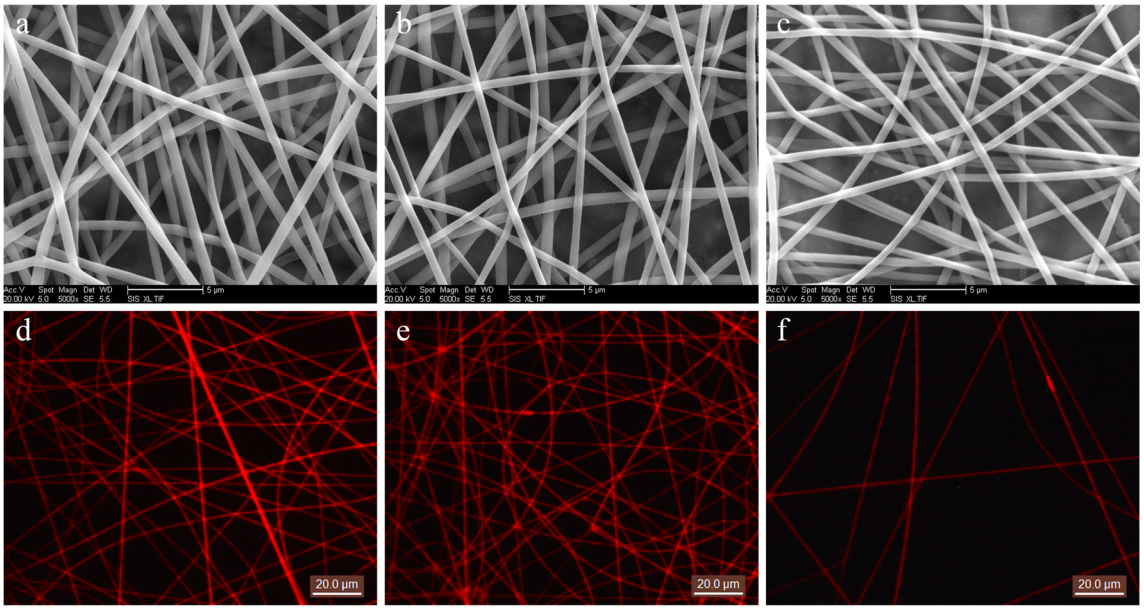

Fig. 1 SEM images (**a**–**c**) show the representative morphological structures of neat PMMA nanofibers and composite nanofibers with $Eu_2(BTP)_3(Phen)_2$ contents of 11 wt% (**b**),13 wt% (**c**), respectively. Fluorescence microscope images (**d**–**f**) show the representative morphological structures of composite nanofibers with $Eu_2(BTP)_3(Phen)_2$ contents of 11 wt% (**d**), 13 wt% (**e**), and 15 wt% (**f**)

Results and discussion

Morphology of composite nanofibers and dispersion of $Eu_2(BTP)_3(Phen)_2$

SEM images of a typical electrospun sheet demonstrated the random distribution of fibers, which reveal that the composite nanofibers consists of $Eu_2(BTP)_3(Phen)_2$ and PMMA with an average diameter of 565±33 nm have been successfully prepared (Fig. 1a–c). The surface of the composite nanofibers is smooth without identifiable particles, suggesting that the $Eu_2(BTP)_3(Phen)_2$ might be uniformly dispersed into the nanofibers.

The images of fluorescence microscope (Fig. 1d–f) show the luminescent intensity reached its maximum at 11 wt% and decreased with the content of $Eu_2(BTP)_3(Phen)_2$ increasing from 11 to 15 wt% with extraordinary red light under ultraviolet irradiation. Additionally, the bright spot in Fig. 1e, f mainly owe to the aggregation of $Eu_2(BTP)_3(Phen)_2$ formed in the electrospinning solutions, leading to the nanoparticles in the resultant composite nanofibers.

FT-IR measurement analysis

FT-IR spectra of PMMA, Eu/PMMA composite fibers, $Eu_2(BTP)_3(Phen)_2$ complex, and BTP (Fig. 2) reveal that the peak at 1735 cm^{-1} is assigned to the C=O stretching band of

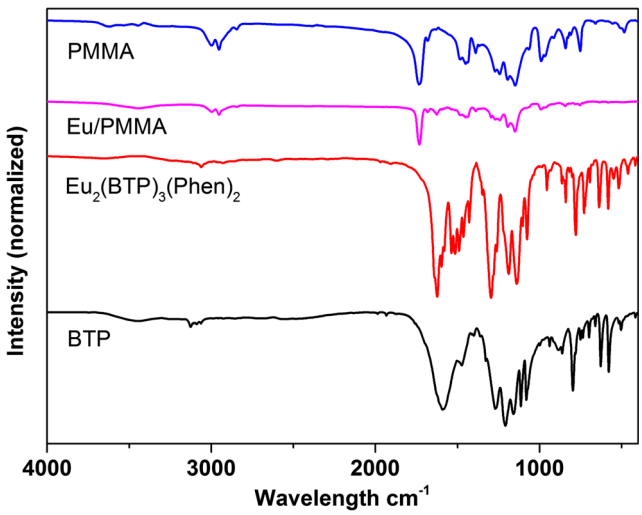

Fig. 2 FT-IR spectra of PMMA fibers, Eu/PMMA fibers, $Eu_2(BTP)_3(Phen)_2$, and BTP

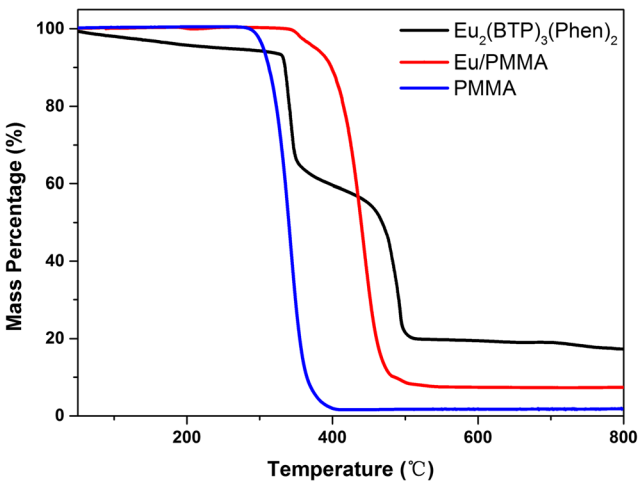

Fig. 3 TGA curves of the complex $Eu_2(BTP)_3(Phen)_2$, Eu/PMMA, and PMMA

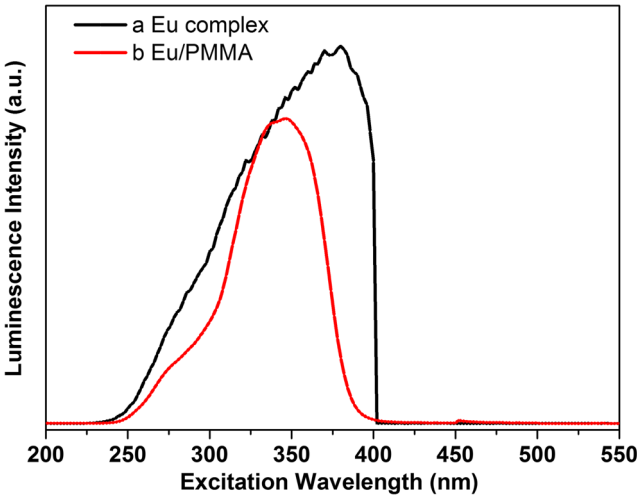

Fig. 4 Excitation spectra of $Eu_2(BTP)_3(Phen)_2$ (**a**) and the composite nanofibers with $Eu_2(BTP)_3(Phen)_2$ (**b**)

PMMA, while this band is red shifted to 1732 cm^{-1} in the Eu/PMMA fibers, which suggests that oxygen atoms of the carbonyl group of PMMA are interacted with Eu^{3+} ions in the complex $Eu_2(BTP)_3(Phen)_2$. The absence of the band in the region of 3000–3500 cm^{-1} implies that H_2O molecules have been substituted by Phen in the complex $Eu_2(BTP)_3(Phen)_2$ and the Eu/PMMA fibers. A weak absorption peak at 1627 cm^{-1} in the Eu/PMMA fibers which was assigned to the overtone of the C=O stretching mode in BTP shows the complex $Eu_2(BTP)_3(Phen)_2$ was successfully doped into PMMA.

Thermal properties of the nanofibers

To determine the thermal stability of the composite fiber samples, the thermogravimetric analysis (TGA) experiments were performed; the results are shown in Fig. 3. The thermal decomposition of the $Eu_2(BTP)_3(Phen)_2$ composite fibers begins at around 346 °C which shows an enhancement of 15 °C for the decomposition temperature (T_d) in comparison with the $Eu_2(BTP)_3(Phen)_2$ complexes. It is also shown that the undoped PMMA polymer fiber decomposes in a one-step event and its degradation starts at 286 °C. Similarly, the PMMA polymer fiber doped with the $Eu_2(BTP)_3(Phen)_2$ complex also presented a curve of decomposition with one single decomposition event. The weight loss of $Eu_2(BTP)_3(Phen)_2$/PMMA composite nanofiber occurs over a wide temperature interval (346–505 °C) which exhibits an increase about 60 °C compared with the undoped PMMA polymer fiber. The improved thermal stability for the Eu/PMMA fibers can be attributed to the chemical bonding between the oxygen atoms of the carbonyl groups in PMMA and the Eu^{3+} ions in $Eu_2(BTP)_3(Phen)_2$. The result also proves that PMMA as polymer matrix can provide an excellent and stable chemical environment for Eu^{3+} complexes, because the rigid chain segments of polymer limit the vibration of organic ligands, enhancing relative independence of the doped molecules.

Effects of complex concentration on the luminescence of nanofibers

The luminescent properties of the solid neat complex of $Eu_2(BTP)_3(Phen)_2$ and the $Eu_2(BTP)_3(Phen)_2$/PMMA composite nanofibers were recorded at room temperature. The excitation spectra for various samples are shown in Fig. 4. The excitation top point is 365 nm in the neat complex of $Eu_2(BTP)_3(Phen)_2$ (Fig. 4) which is blue shifted and split into two bands centered at 335 and 346 nm in the $Eu_2(BTP)_3(Phen)_2$/PMMA nanofibers. This indicated that the site symmetry of the Eu^{3+} ions in the complex composite nanofibers was lower than that of the Eu^{3+} ions in the neat complex $Eu_2(BTP)_3(Phen)_2$ for the influences of the

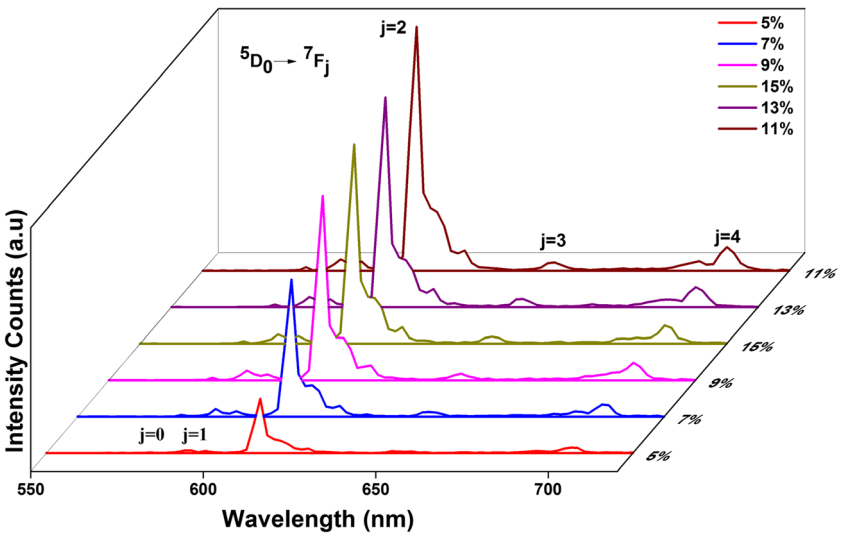

Fig. 5 Emission spectra (λ_{ex}= 335 nm) of the composite nanofibers with $Eu_2(BTP)_3(Phen)_2$ contents of 5, 7, 9, 11, 13, and 15 wt%

Table 1 Solid-state spectroscopic parameters for the $^5D_0$ luminescence of the $Eu_2(BTP)_3(Phen)_2$ complex and the $Eu_2(BTP)_3(Phen)_2$/PMMA nanofibers

Samples	I_{02}/I_{01}	Ω_2	Ω_4	A_{RAD} (s^{-1})	A_{NR} (s^{-1})	τ_{obs} (μs)	Φ(%)
$Eu_2(BTP)_3(Phen)_2$	7.32	17.31	3.87	857	246	906	65
A[a]	14.24	20.01	5.44	871	912	561	31
B	13.34	18.85	5.11	817	981	556	29
C	13.10	18.55	5.03	804	1141	514	27

[a] The samples A, B, and C are the composite nanofibers with $Eu_2(BTP)_3(Phen)_2$ contents of 11, 13, and 15 wt%, respectively

neighboring chain segments of PMMA [22]. Additionally, both $^7F_0 \rightarrow {}^5D_2$ and $^7F_1 \rightarrow {}^5D_1$ excitations for the composite nanofibers disappeared, suggesting that the f→f inner-shell transitions for the composite nanofibers were quenched via non-radiative energy transfers [23]. However, the luminescent intensity of the $Eu_2(BTP)_3(Phen)_2$/PMMA nanofibers decreased when the content of $Eu_2(BTP)_3(Phen)_2$ was over 11 wt%, indicating that the nanoparticles of $Eu_2(BTP)_3(Phen)_2$ in the PMMA matrices start to aggregate slightly. This was mainly because the $Eu_2(BTP)_3(Phen)_2$ predominantly existed as molecular clusters and/or nanoparticles when the content of the complex was high enough. During electrospinning, the solutions contain uniformly dispersed $Eu_2(BTP)_3(Phen)_2$ molecules and the rapid evaporation of the solvent concomitant fast solidification of the filaments (within tens of milliseconds) hindered the aggregation of $Eu_2(BTP)_3(Phen)_2$ [24].

In the emission spectra (Fig. 5), the peak intensities at 580, 590, 612, 652, and 701 nm were assigned to the J=0, 1, 2, 3, and 4 transitions, respectively. Additionally, the $^5D_0 \rightarrow {}^7F_2$ hypersensitive transition at 612 nm originated from the Eu^{3+} ions was the most intense emission, suggesting there was a highly polarized chemical environment around the Eu^{3+} ions [25].

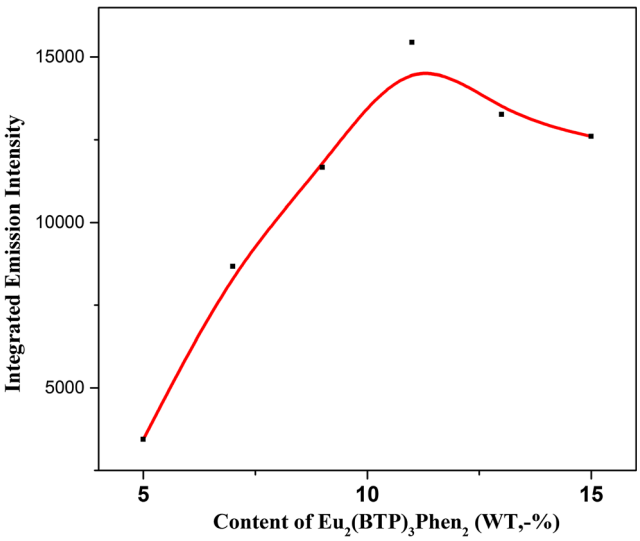

Fig. 6 Correlation of the integrated emission intensity for $^5D_0 \rightarrow {}^7F_2$ transitions of Eu^{3+} ions versus the $Eu_2(BTP)_3(Phen)_2$ content in the composite nanofibers

The intensity ratios (I_{02}/I_{01}) between the electric dipole transition ($^5D_0 \rightarrow {}^7F_2$) and the magnetic dipole transition ($^5D_0 \rightarrow {}^7F_1$), a measure of the asymmetry of the local environment of Eu^{3+} ions [26], are shown in Table 1. It is worth mentioning that the ratio of the neat $Eu_2(BTP)_3(Phen)_2$ is almost only half of that of the composite nanofibers. This suggests that the symmetry of the coordination sphere for the Eu^{3+} ions was more disordered, and the degree of polarization was higher in the composite fibers as compared to the pure $Eu_2(BTP)_3(Phen)_2$, which further led to higher probability for the electronic dipole-allowed transitions [27].

Figure 6 shows the integrated emission intensity of the electric dipole transition ($^5D_0 \rightarrow {}^7F_2$) as a function of the $Eu_2(BTP)_3(Phen)_2$ content in the composite nanofibers. The emission intensity enhanced with increasing content of the $Eu_2(BTP)_3(Phen)_2$ and reached its maximum value at 11 wt%. The further intensity decreased with the increasing content of the complex because of typical emission concentration quenching which was due to the deactivation of the $^5D_0$ and $^5D_1$ states through the electrostatic multipolar interactions and the exciton migration through the Foürster dipole-dipole mechanism. The mechanism has been illustrated in the Supporting Material. The electrospun composite nanofibers, compared with the composite polymers prepared by copolymerization, achieved higher contents without inducing the concentration quenching owing to the desired dispersion of $Eu_2(BTP)_3(Phen)_2$ in the matrix of the composite nanofibers

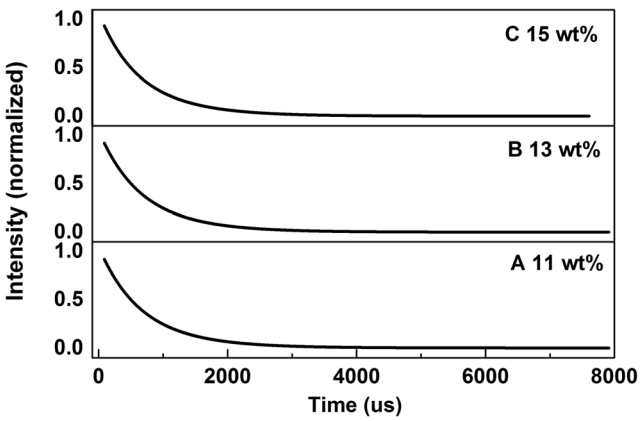

Fig. 7 Luminescence decay curves of the excited Eu^{3+} ions at the $^5D_0$ level for composite nanofibers with $Eu_2(BTP)_3(Phen)_2$ contents of 11 to 15 wt%

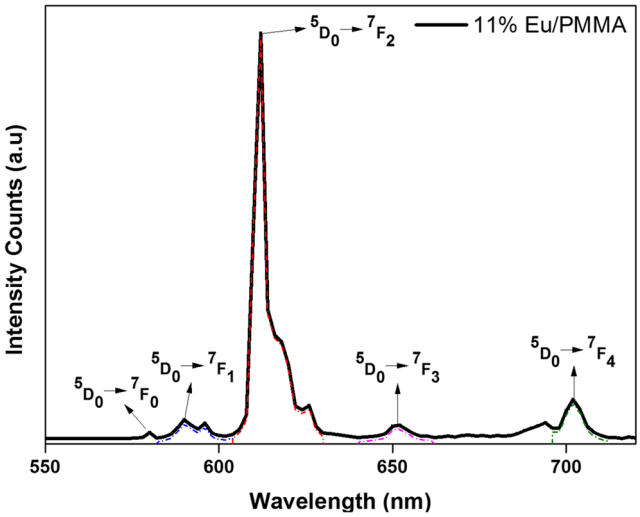

Fig. 8 The high-resolution emission spectrum of the composite nanofiber with $Eu_2(BTP)_3(Phen)_2$ contents of 11 wt%

might be even more preferred than the distribution of $Eu_2(BTP)_3(Phen)_2$ units along macromolecular chains [28]. On one hand, when the content of $Eu_2(BTP)_3(Phen)_2$ was low in the composite nanofibers, most of $Eu_2(BTP)_3(Phen)_2$ dispersed as molecular states and/or nanoparticles and the exciton migration through the diffusion-induced collision among Eu^{3+} ions was negligible. On the other hand, when the content of $Eu_2(BTP)_3(Phen)_2$ was high, some aggregates with sizes of tens of nanometers formed, which led to high Eu^{3+} ion concentrations locally and were responsible for the emission concentration quenching [29].

Judd-Ofelt analysis and luminescent quantum efficiency

The Judd-Ofelt theory is a widely accepted tool for exploring f→f inner shell electronic transitions in Ln^{3+} complexes [30]. The Judd-Ofelt parameters Ω_λ (λ=2, 4, and 6) are interaction parameters of ligand fields, in which Ω_2 is sensitive to the chemical microenvironment around the Eu^{3+} ions [31]. The values of Ω_2 and Ω_4 can be estimated from the oscillator strengths of the $^5D_0 \rightarrow {}^7F_2$ and $^5D_0 \rightarrow {}^7F_4$ transitions in the emission spectrum (Fig. 5), using the magnetic dipole transition of $^5D_0 \rightarrow {}^7F_1$ as the reference [32] (Fig. 7). Table 1 presents the Judd-Ofelt intensity parameters (Ω_2, Ω_4), radiative transition rate (A_{RAD}), non-radiative transition rate (A_{NR}), fluorescence lifetime (τ_{obs}), and luminescence quantum efficiency (Φ) for the $^5D_0$ state of the Eu^{3+} ions in the neat

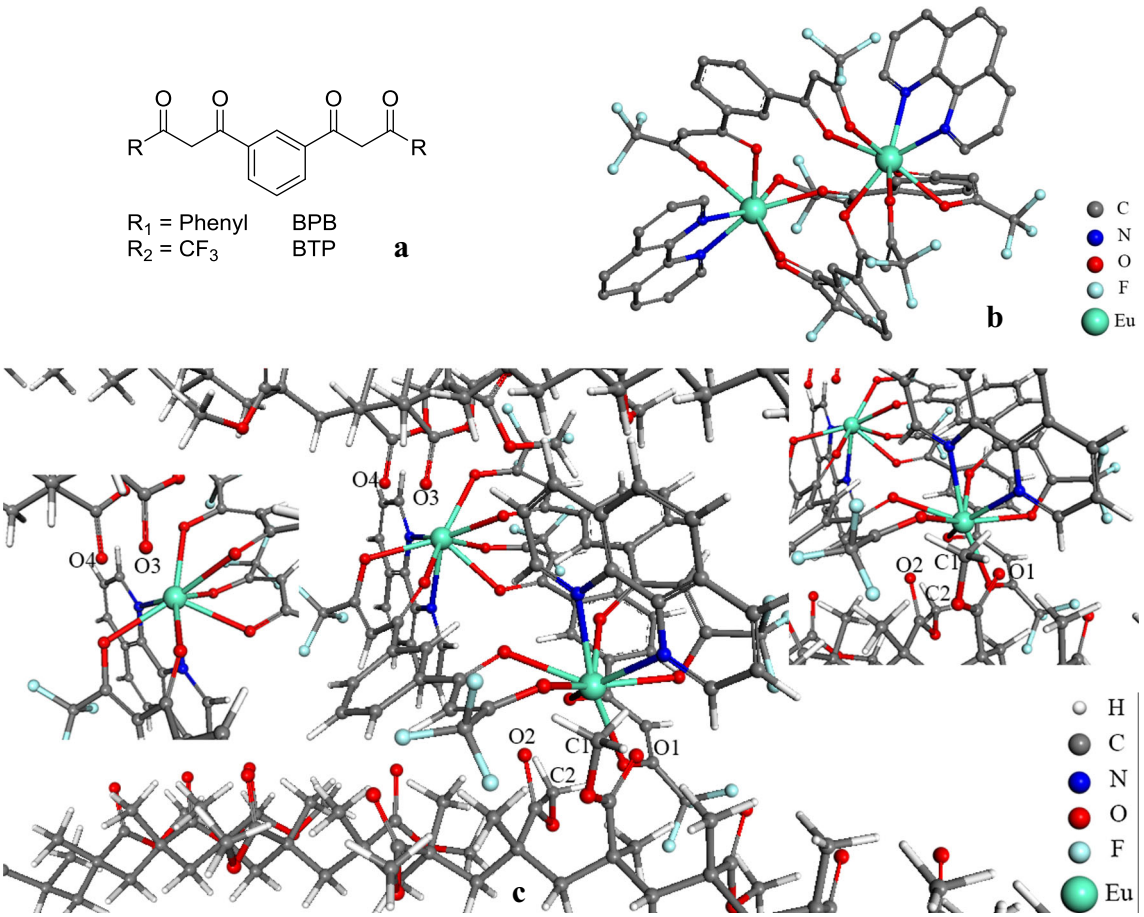

Fig. 9 Molecular structures of BPB and BTP (**a**), molecular model of $Eu_2(BTP)_3(Phen)_2$ (**b**) and Eu/PMMA (**c**)

complex $Eu_2(BTP)_3(Phen)_2$ and the composite nanofibers. The high-resolution emission spectrum of the composite nanofiber with $Eu_2(BTP)_3(Phen)_2$ contents of 11 wt% (Fig. 8) is given to determine the integrated area of $^5D_0 \rightarrow {}^7F_J$ (J=1, 2, 3, and 4) transition. The large values of Ω_2 might be interpreted as a consequence of the hypersensitive behavior of the $^5D_0 \rightarrow {}^7F_2$ transition [33] which suggests that the chemical environment of the Eu^{3+} ions is highly polarizable. The Ω_4 parameter values, less sensitive to the coordination environment than Ω_2, reflect a rigid chemical environment surrounding the Eu^{3+} ions [34]. The specific calculations and detailed principles were provided in the Supporting Material. The higher Ω_2 values of the composite nanofibers than that of the neat $Eu_2(BTP)_3(Phen)_2$ suggested an enhancement of the $^5D_0 \rightarrow {}^7F_2$ hypersensitive transition [35]. This was also attributed to the change of the chemical environment surrounding Eu^{3+} ions, which was induced by the intermolecular interactions between neighboring chain segments of PMMA and $Eu_2(BTP)_3(Phen)_2$ [36]. The higher values of Ω_4 for the composite nanofibers as compared with that of the neat $Eu_2(BTP)_3(Phen)_2$ indicated a perturbation on the coordination effect of the bis-bidentate BTP by the steric factors from the surrounding PMMA.

Furthermore, with increasing content of the $Eu_2(BTP)_3(Phen)_2$, the values of Ω_2 and Ω_4 decreased, suggesting that the effect of neighboring PMMA chain segments on the ligand fields of Eu^{3+} were gradually weakened. Such a phenomenon was attributed to the uniform dispersion of $Eu_2(BTP)_3(Phen)_2$ in the nanofiber matrix. When the content of $Eu_2(BTP)_3(Phen)_2$ was lower than 13 wt%, most of the $Eu_2(BTP)_3(Phen)_2$ existed as molecular complex and the chemical environment around the Eu^{3+} ions was significantly affected by the surrounding PMMA, whereas such an influence reduced gradually with the increase of the complex content resulting in the formation of aggregates [37].

Simulative microchemical environment of Eu^{3+} ions in fiber

Two bis-β-diketone ligands, 1,3-bis(3-phenyl-3-oxopropanoyl)benzene (BPB) [38] and BTP, which bear two conjugated diketonate binding sites linked by a 1,3-phenylene spacer (Fig. 9a), were published. The molecular structures of the bis-β-diketone Eu^{3+} complexes represent with molecular models as neutral triple-stranded dinuclear lanthanide helices. The construction of the $Eu_2(BTP)_3(Phen)_2$ complex model was based on the $Eu_2(BTP)_3bpy_2$ complex crystal structure [21], and no solvent molecules were considered. In the structure of the model 1 (Fig. 9b), each central Eu^{3+} ion is coordinated with six oxygen atoms from three BTP ligands and two nitrogen atoms from Phen. Because of different molecular structure of the $Eu_2(BTP)_3(Phen)_2$ complex in PMMA, the quantum efficiency of Eu/PMMA is lower than that of the pure complex (Table 1). The diverse steric configurations of the hybrid complex (Fig. 9c) are because the steric hindrance caused by the tremendous polymeric structure in such a short unit of the carbon chains, which could increase the level of non-radiative transition rate and restrict the efficiency of the intramolecular transfer mechanism. Specifically, in Fig. 9c, two groups of ester carbonyls were attracted by two Eu^{3+} ions and insert the space of $Eu_2(BTP)_3(Phen)_2$. One of them (O3 and O4) has less influence on the structure of $Eu_2(BTP)_3(Phen)_2$ than another (O1 and O2), because there is no methyl or other group of PMMA in the space of the complex. On the other hand, not only two ester carbonyls, but also two methyls (C1 and C2) are located on the same monomer, respectively. In such a microscopic structure, the distance of CH should be considered. Both C1 and C2 can influence the steric configuration of the complex by steric hinder.

Conclusion

In summary, we had successfully fabricated $Eu_2(BTP)_3(Phen)_2$/PMMA nanofibers with great thermal stability by electrospinning. The microstructure of the fibers, obtained by SEM, showed the preparation of continuous fibers with a homogeneous morphology and an average diameter of 565± 33 nm. Fluorescence spectra and Judd-Ofelt parameters indicated that the $Eu_2(BTP)_3(Phen)_2$/PMMA nanofibers had a maximum luminescence intensity at the content of 11 wt%. Meanwhile, spectroscopic parameters (Ω_2, Ω_4, A_{RAD}, and A_{NR}) analysis suggested that the increase of polarization degree and the enhancement of the electronic dipole-allowed transitions of Eu^{3+} ions were caused by the interactions between the $Eu_2(BTP)_3(Phen)_2$ molecules and neighboring chain segments of PMMA. In addition, the thermal stability of the composite nanofibers was much better than that of the pure complex $Eu_2(BTP)_3(Phen)_2$ because of the addition of the polymer matrixes. This study provide a new and useful way in the fabrication of innovative composite nanomaterial containing luminescent bis-β-diketone Eu^{3+} complexes, and the development of 1D nanomaterials could find important applications, especially in optical communications and luminescent probes.

Acknowledgments We are grateful for the financial support by the National Natural Science Foundation of China (No. 51303045) and the Education Department of Heilongjiang Province of China (No. 12521413).

References

1. Bünzli J-CG (2010) Lanthanide luminescence for biomedical analyses and imaging. Chem Rev 110:2729–2755
2. Woodward AW, Frazer A, Morales AR, Yu J, Moore AF, Campiglia AD, Jucov EV, Timofeeva T, Belfield KD (2014) Two-photon

sensitized visible and near-IR luminescence of lanthanide complexes using a fluorene-based donor-π-acceptor diketonate. Dalton Trans 43:16626
3. Park H-J, Ko S-B, Wyman IW, Wang S (2014) Selective sensitization of Eu(III) and Tb(III) emission with triarylboron-functionalized dipicolinic acids. Inorg Chem 53:9751
4. D'Aléo A, Pointillart F, Ouahab L, Andraud C, Maury O (2012) Charge transfer excited states sensitization of lanthanide emitting from the visible to the near-infra-red. Coord Chem Rev 256:1604
5. Kai J, Felinto MC, Nunes LA, Malta OL, Brito HF (2011) Intermolecular energy transfer and photostability of luminescence-tuneable multicolour PMMA films doped with lanthanide-β-diketonate complexes. J Mater Chem 21:3796–3802
6. Li D, Tian X, Hu G, Zhang Q, Wang P, Sun P, Tian Y (2011) Synthesis, crystal structures, photophysical properties, and bioimaging of living cells of Bis-β-diketonate phenothiazine ligands and its cyclic dinuclear complexes. Inorg Chem 50:7997
7. Freund C, Porzio W, Giovanella U, Vignali F, Pasini M, Destri S, Mech A, Di Pietro S, Di Bari L, Mineo P (2011) Thiophene based europium β-diketonate complexes: effect of the ligand structure on the emission quantum yield. Inorg Chem 50:5417
8. Feng J, Zhang H (2013) Hybrid materials based on lanthanide organic complexes: a review. ChemSoc Rev 42:387
9. Hudson ZM, Sun C, Helander MG, Chang Y-L, Lu Z-H, Wang S (2012) Highly efficient blue phosphorescence from triarylboron-functionalized platinum(II) complexes of N-heterocyclic carbenes. J Am Chem Soc 134:13930
10. Chen X-Y, Yang X, Holliday BJ (2008) Photoluminescent europium-containing inner sphere conducting metallopolymer. J Am Chem Soc 130:1546
11. Peng H, Stich MIJ, Yu J, L-n S, Fischer LH, Wolfbeis OS (2010) Luminescent europium(III) nanoparticles for sensing and imaging of temperature in the physiological range. Adv Mater 22:716
12. Leong WL, Vittal JJ (2010) One-dimensional coordination polymers: complexity and diversity in structures, properties, and applications. Chem Rev 111:688
13. Xie JL, Guo CX, Li CM (2014) Construction of one-dimensional nanostructures on graphene for efficient energy conversion and storage. Energy Environ Sci 7:2559
14. Martin CR (1994) Nanomaterials: a membrane-based synthetic approach. Science 266:1961
15. Law M, Goldberger J, Yang P (2004) Semiconductor nanowires and nanotubes. Annu Rev Mater Res 34:83
16. Hartgerink JD, Beniash E, Stupp SI (2001) Self-assembly and mineralization of peptide-amphiphile nanofibers. Science 294:1684
17. Park J, Karim M, Kim I, Cheong I, Kim J, Bae D, Cho J, Yeum J (2010) Electrospinning fabrication and characterization of poly(vinyl alcohol)/montmorillonite/silver hybrid nanofibers for antibacterial applications. Colloid Polym Sci 288:115
18. Hu X, Liu S, Zhou G, Huang Y, Xie Z, Jing X (2014) Electrospinning of polymeric nanofibers for drug delivery applications. J Contr Release Off J Contr Release Soc 185:12
19. Kuriki K, Koike Y, Okamoto Y (2002) Plastic optical fiber lasers and amplifiers containing lanthanide complexes. Chem Rev 102: 2347
20. Bassett AP, Magennis SW, Glover PB, Lewis DJ, Spencer N, Parsons S, Williams RM, De Cola L, Pikramenou Z (2004) Highly luminescent, triple- and quadruple-stranded, dinuclear Eu, Nd, and Sm(III) lanthanide complexes based on Bis-diketonate ligands. J Am Chem Soc 126:9413
21. Shi J, Hou Y, Chu W, Shi X, Gu H, Wang B, Sun Z (2013) Crystal structure and highly luminescent properties studies of bis-β-diketonate lanthanide complexes. Inorg Chem 52:5013
22. Moudam O, Rowan BC, Alamiry M, Richardson P, Richards BS, Jones AC, Robertson N (2009) Europium complexes with high total photoluminescence quantum yields in solution and in PMMA. Chemical Communications 6649
23. Ravi Kumar V, Veeraiah N, Appa Rao B, Bhuddudu S (1998) Optical absorption and photoluminescence properties of Eu^{3+}-doped ZnF_2–PbO–TeO_2 glasses. J Mater Sci 33:2659
24. Wang S-J, Hu J-B, Wang Y-Y, Luo F (2013) Coating graphene oxide sheets with luminescent rare-earth complexes. J Mater Sci 48:805
25. Francis B, Ambili Raj DB, Reddy MLP (2010) Highly efficient luminescent hybrid materials covalently linking with europium(iii) complexes via a novel fluorinated β-diketonate ligand: synthesis, characterization and photophysical properties. Dalton Trans 39: 8084
26. Qi S, Huang Y, Li Y, Cai P, Kim SI, Seo HJ (2014) Probe spectrum measurements of Eu^{3+} ions as a relevant tool for monitoring in vitro hydroxyapatite formation in a new borate biomaterial. J Mater Chem B 2:6387
27. Kai J, Parra DF, Brito HF (2008) Polymer matrix sensitizing effect on photoluminescence properties of Eu^{3+}-β-diketonate complex doped into poly-β-hydroxybutyrate (PHB) in film form. J Mater Chem 18:4549
28. Lima AC, Sher P, Mano JF (2012) Production methodologies of polymeric and hydrogel particles for drug delivery applications. Expert Opin Drug Deliv 9:231
29. Smirnov VA, Sukhadolski GA, Philippova OE, Khokhlov AR (1999) Use of luminescence of europium ions for the study of the interaction of polyelectrolyte hydrogels with multivalent cations. J Phys Chem B 103:7621
30. Chau PTM, Ryu KH, Yo CH (1998) Influence of the technological conditions on the luminescence of Eu^{3+} ions in Sr_2SnO_4. J Mater Sci 33:1299
31. Wada A, Watanabe M, Yamanoi Y, Nishihara H (2008) Modification of the luminescence spectra of chloro (tetrapyridylcyclotetramine) europium complexes by fine tuning of the Eu-Cl distance with outer-sphere counterions in the solid state, in a polymer matrix and in solution. Chemical Communications 1671
32. Carlos LD, Messaddeq Y, Brito HF, Sá Ferreira RA, de Zea BV, Ribeiro SJL (2000) Full-color phosphors from europium(III)-based organosilicates. Adv Mater 12:594
33. Görller-Walrand C, Fluyt L, Ceulemans A, Carnall WT (1991) Magnetic dipole transitions as standards for Judd-Ofelt parametrization in lanthanide spectra. J Chem Phys 95:3099
34. Divya V, Freire RO, Reddy MLP (2011) Tuning of the excitation wavelength from UV to visible region in Eu^{3+}-β-diketonate complexes: comparison of theoretical and experimental photophysical properties. Dalton Trans 40:3257
35. Liu X, Hu Y, Wang B, Su Z (2009) Synthesis and fluorescent properties of europium–polymer complexes containing 1,10-phenanthroline. Synth Met 159:1557
36. Zhang X, Wen S, Hu S, Chen Q, Fong H, Zhang L, Liu L (2010) Luminescence properties of Eu(III) complex/polyvinylpyrrolidone electrospun composite nanofibers. J Phys Chem C 114:3898
37. Tian Y, Chen B, Li X, Zhang J, Tian B, Sun J, Cheng L, Zhong H, Zhong H, Hua R (2012) Solvothermal synthesis and tunable luminescence of Tb^{3+}, Eu^{3+} codoped YF_3 nano- and micro-crystals with uniform morphologies. J Solid State Chem 196:187
38. Bassett AP, Magennis SW, Glover PB, Lewis DJ, Spencer N, Parsons S, Williams RM, De Cola L, Pikramenou Z (2004) Highly luminescent, triple-and quadruple-stranded, dinuclear Eu, Nd, and Sm (III) lanthanide complexes based on bis-diketonate ligands. J Am Chem Soc 126:9413